HHS Public Access

Author manuscript

Biosens Bioelectron. Author manuscript; available in PMC 2022 November 15.

Published in final edited form as:

Biosens Bioelectron. 2021 November 15; 192: 113479. doi:10.1016/j.bios.2021.113479.

Come together: on-chip bioelectric wound closure

Tom J. Zajdel[a], **Gawoon Shim**[a], **Daniel J. Cohen**[a]

[a]Mechanical & Aerospace Engineering, Princeton University, 08544 Princeton, New Jersey, United States

Abstract

There is a growing interest in bioelectric wound treatment and electrotaxis, the process by which cells detect an electric field and orient their migration along its direction, has emerged as a potential cornerstone of the endogenous wound healing response. Despite recognition of the importance of electrotaxis in wound healing, no experimental demonstration to date has shown that the actual closing of a wound can be accelerated solely by the electrotaxis response itself, and *in vivo* systems are too complex to resolve cell migration from other healing stages such as proliferation and inflammation. This uncertainty has led to a lack of standardization between stimulation methods, model systems, and electrode technology required for device development. In this paper, we present a 'healing-on-chip' approach that is a standardized, low-cost, model for investigating electrically accelerated wound healing. Our device provides a biomimetic convergent field geometry that more closely resembles actual wound fields. We validate this device by using electrical stimulation to close a 1.5 mm gap between two large (30 mm^2) layers of primary skin keratinocyte to completely heal the gap twice as quickly as in an unstimulated tissue. This demonstration proves that convergent electrotaxis is both possible and can accelerate healing and offers an accessible 'healing-on-a-chip' platform to explore future bioelectric interfaces.

Keywords

Bioelectricity; wound healing; cell migration; electrotaxis; bioengineering

1. Introduction

Since du Bois-Reymond first characterized the naturally occurring 'wound current' nearly two centuries ago (Bois-Reymond, 1848), there has been significant interest in applying external electrical stimulation to improve wound healing (Anderson et al., 2016; Hunckler and De Mel, 2017; Tai et al., 2018). The potential for this approach is becoming increasingly apparent, with the pressing need for new technologies to expedite and improve wound care

Corresponding Author: Daniel J. Cohen, danielcohen@princeton.edu, 109 Hoyt Laboratory, Princeton, NJ 08544.

Authorship contribution statement

Tom J. Zajdel: Methodology, Software, Formal Analysis, Visualization, Investigation, Writing – Original Draft

Gawoon Shim: Validation, Investigation, Writing—Review & Editing

Daniel J. Cohen: Conceptualization, Methodology, Writing – Original Draft/Review & Editing, Supervision, Project Administration, Resources, Funding acquisition

Declaration of competing interest

The authors declare that they have no known competing financial interests or personal relationships that could have appeared to influence the work reported in this paper.

given increasing prevalence and healthcare burden of wound treatments (Martinengo et al., 2019; Padula and Delarmente, 2019)

There is growing evidence from *in vitro* and *in vivo* studies that electrical stimulation has therapeutic potential. Improvement in skin healing in animal models upon electric field stimulation has been demonstrated in recent years (Jang et al., 2018; Kai et al., 2017; Liang et al., 2020; Long et al., 2018; Wang et al., 2020; Yu et al., 2019), while clinical research on human subjects using electrical stimulation to treat chronic wounds such as pressure ulcers, ischemic wounds, and diabetic wounds also reported varying levels of success (Franek et al., 2012; Kloth, 2014, 2005; Morris, 2006; Ud-Din and Bayat, 2014). Commercial products are available for wound clinics (ACP, 2017; Ovens, 2014) and recent clinical guidelines now include evaluations and recommendations for electrical stimulation treatment for pressure ulcers (Haesler, 2014).

However, despite the promising outlook, bioelectric wound therapy is far from the standard of care. This discrepancy is due to broad gaps in both technology development and biological knowledge describing how electrical stimulation may act to improve wound healing. Technologically, optimum stimulation parameters for field strength, biointerface design, and current delivery mode remain unclear (Khouri et al., 2017; Zhao et al., 2014). Biologically, there is uncertainty about how the key wound healing mechanisms--cell migration, proliferation, and inflammation—are affected by electric stimulation (Tai et al., 2018). This ambiguity has resulted in a lack of standardization in stimulation schemes, model systems, and technology that can all lead to issues of reproducibility and lengthy design iterations that have slowed progress (Ashrafi et al., 2017; Isseroff and Dahle, 2012; Kloth, 2005). Furthermore, there have been very few experimental designs that allowed close observation of directed cellular motion and its role in wound healing. *In vivo* and clinical studies that use a central cathode and peripheral anode mainly use pulsed or biphasic electrical currents instead of direct current, targeting other aspects of the wound response instead of directed cellular motion (Kai et al., 2017; Kloth, 2014). Moreover, these methodologies are not compatible with live imaging of the cellular response.

Here, we begin to address this problem by integrating a popular technical approach used in other branches of biotechnology—'organ-on-a-chip' systems—to reduce the complexity of biomedical problems for increased tractability and translatability. Organ-on-a-chip (OoC) platforms are model systems that capture a specific and critical physiological behavior of the *in vivo* system in a standardized, rapid, lower-cost *in vitro* model. To date, OoCs have clearly proven their value in other fields by aiding discoveries and treatments for lung, gut, and vascular pathologies (Wang et al., 2015; Zhang and Radisic, 2017; Zhang et al., 2018). Here, we use an OoC approach to integrate a 'healing-on-a-chip' platform with a custom electrobioreactor designed from the ground up to investigate electrically accelerated wound healing.

While there are many effects that applied electrical stimulation may have on tissue growth and healing, one of the most well-characterized is electrotaxis—the directed motion of cells in response to an electric current. The mechanism of current detection is thought to be electrophoresis of charged membrane-bound receptors in the presence of an electric field,

resulting in an asymmetric distribution of these proteins that triggers downstream signaling of the cell migration machinery (Allen et al., 2013). Electrotaxis is seen in over 20 cell types across multiple organisms where cells sense and track electrochemical potential gradients (~1 V/cm) that emerge during development and injury healing (Cortese et al., 2014; Kennard and Theriot, 2020; McCaig et al., 2009). *In vivo*, these fields result in negative polarization of the center of a skin wound relative to the periphery of the wound (Shen et al., 2016; Wahlsten et al., 2016). Direct current fields are analogous to fields *in vivo* (McCaig et al., 2005), in contrast to the pulsed DC or AC stimulation used in many *in vivo* studies (Hunckler and De Mel, 2017; Long et al., 2018), and are sufficient to induce the electrotaxis response as shown in *in vitro* assays that demonstrated control of cells and simple tissues using spatially programmed electric cues (Cohen et al., 2014; Gokoffski et al., 2019; Zajdel et al., 2020). Given the ubiquity of electrotaxis and the sensitivity of cell migration to electrical cues, electrotaxis likely plays a significant role in the reepithelialization stage of wound healing, and perhaps other phases.

However, at present there is no study, either *in vitro* or *in vivo* that conclusively indicates that electrotaxis itself can accelerate wound closure to completion as electrotaxis has primarily been studied in isolated single cells to elucidate the molecular biology of the process. This gap stems from the technological limitations of current devices used to study electrotaxis. Nearly all devices use a single electrode pair to apply a uniform, unidirectional field across tissues—such a field would cause one side of a wound to close and the other side to worsen. To our knowledge, there is only one prior convergent field study that reports accelerated wound edge migration (Sun et al., 2012), although this study focused on fibroblasts and provided stimulation for 2 hrs, which was insufficient to actually close the wound model, hence further investigation is warranted. In addition, most studies and devices do not generalize well to macroscale tissues and wounds since precise tissues with reproducible, millimetric wounds must be grown inside the electrobioreactor. Finally, macroscale cell migration requires stable electrical stimulation over many hours, and the common, bleach-based electrode preparation process is insufficient for long-term stimulation (>4 hours). An ideal bioelectric ‘wound-on-a-chip’ platform should address these issues.

Here we build on our prior work (Cohen et al., 2014; Zajdel et al., 2020) to create a new electrobioreactor to study healing in a macroscale skin-on-a-chip model using primary mouse skin monolayers which migrate toward the cathode when stimulated (Figure 1), and to use electrical stimulation to accelerate closure of 1.5 mm large model skin wounds by at least 2X over unstimulated skin layers (Figures 2, 3). To accomplish this, we developed electrotaxis infrastructure specifically designed to recapitulate the constraints of wound healing, delivering a sustained converging electric field to a tissue (Figure 1). With this device, we were able to engineer and stimulate the largest tissues yet tested with electrotaxis (30 mm^2) for 12 hours, while also exploring the consequences of continuing stimulation beyond the point of wound closure and tissue collision.

2. Material and Methods

2.1. Cell Culture

Primary keratinocytes were originally harvested from mice (courtesy of the Devenport Laboratory, Princeton University). Cells were cultured in E-medium supplemented with 15% serum and 50 μM calcium and maintained at 37 °C under 5% CO2 and 95% relative humidity. Cells were split before reaching 70% confluence and a given sample was used only for 15-30 passages.

2.2. Device fabrication and assembly

This device assembly is a modified version of the SCHEEPDOG bioreactor from our prior work, and our methods are similar to those published previously (Zajdel et al., 2020). The chamber geometry was designed in vector graphics software (Affinity Designer) and then simulated in finite element software (COMSOL) to predict the field geometry. The stencil defining the pattern was cut from a 250 μm thick sheet of silicone rubber (Bisco HT-6240, Stockwell Elastomers) by a computer-controlled cutter (Cameo, Silhouette). This stencil was applied to a 10 cm tissue culture dish (Falcon) and formed the outline of the electro-stimulation zone. Fibronectin was adsorbed to the dish's surface to provide a matrix for cellular adhesion (protein was dissolved to 50 μg/mL in DI water, applied to the dish for 30 min at 37 °C, then rinsed three times with DI water). A second silicone stencil defined two 3x10 mm microwells, and 10 μL of a seeding solution of cells (singulated keratinocytes suspended in media at a density of 2.0×10^6 cells/ mL) was added to each well. Cells were left to settle for 6 hours in a humidified chamber at 37 °C. After this settling period, the dish was filled with 10 mL of media and incubated for 14 hours to form confluent monolayers.

The three acrylic pieces comprising the reusable device insert were laser milled (VLS 3.5, Universal Laser Systems) out of a 5.2 mm thick acrylic sheet. These individual layers of acrylic were stacked, clamped and solvent welded together with acrylic cement (SCIGRIP 4, SCIGRIP Assembly Adhesives) and set for 24 h. The lid cap for the assembly was cut from a 3 mm thick acrylic sheet and a self-adhesive 1 mm-thick silicone sheet was adhered to one side to provide a better seal against the device insert. All components were sterilized by exposure to 5 min UV radiation in a cell culture hood just before assembly.

After the cell incubation period, the stencil was removed, and the device was assembled immediately. To fabricate the integrated salt bridges, 4% w/v agarose was melted into phosphate buffered saline pH 7.4 on a hot plate. Once fully melted, the agarose was cast into the three slots in the acrylic device to serve as bridges. Once the agarose bridges had solidified, 5-10 mL of PBS was added to each of the three saline reservoirs associated with the agarose bridges. Then, the device was inserted into the tissue culture dish and clamped against the silicone stencil using four modified C-clamps (Humboldt Manufacturing Co.), taking care to avoid trapping air bubbles. Next, the chloridized silver electrodes were inserted into the lid cap and pressed against the acrylic device, so each electrode rested within a separate saline reservoir. Then, a Ti-wire recording electrode was inserted into each well, until it contacted one of the agarose bridges. The completed assembly was then moved to the microscope for imaging.

2.3. Electrode Preparation and Characterization

The silver chloride electrodes used in convergent wound healing assays were prepared by electroplating silver chloride onto silver foil electrodes. To prepare them, silver foil electrodes were immersed in 0.1 M KCl and poised at 3-5 V against a titanium wire counter electrode to a target current density of 1 mA/cm^2 and plated for 14-16 hours. Bleach immersion electrodes were prepared for the basis of comparison by submerging clean silver foil in a commercial 8% bleach solution for 24 hours.

We characterized the cathodic performance of these electrode materials by using a potentiostat to sweep five sequential cyclic voltammetry (CV) cycles in a three-cell electrochemical cell. The working electrode was 3 cm^2 of the cathode material under test, the counter electrode was a 15 cm^2 silver chloride foil, and the reference was a standard Ag/AgCl reference (SYC Technologies, Inc.). Normal operating conditions in our device show a cathodic potential of −1.5 to −1.7 V vs. Ag/AgCl when delivering a current of 6-8 mA, so voltage was swept from 0 to −2 V vs. Ag/AgCl.

2.4. Instrumentation

Two Keithley source meters (Keithley 2400/2450, Tektronix) supplied current to the stimulation electrodes, and both sources shared the central cathode. A USB oscilloscope (Analog Discovery 2, Digilent Inc.) measured the chamber voltage at the Ti recording electrodes, and both meters shared the central probe. A custom MATLAB script adjusted the output currents using proportional feedback control to maintain the desired field strength, and stimulation between the two pairs were alternated every 30 seconds so only one source was active at a given time.

2.5. Microscopy

Time lapse images were acquired on an automated Zeiss (Observer Z1) inverted fluorescence microscope equipped with an XY motorized stage controlled by Slidebook (Intelligent Imaging Innovations, 3i). The microscope was fully incubated at 37 °C within a polycarbonate enclosure. A peristaltic pump (Instech Laboratories) inside the chamber perfused fresh media through the electro-bioreactor at a rate of 2 mL/h. Polyolefin tubing with 1/32” inner diameter and 3/32” outer diameter (Flexelene™, United States Plastic Corp.) conducted media from the pump to the device. This tubing was connected to the acrylic device via a contact fit with a 2.0 mm inlet/outlet access holes cut in the device lid. To regulate media pH, 5% CO_2 was continuously bubbled through the media reservoir. All imaging used a 5X/0.16 fluorescence objective. Cells were either labeled by a lipophilic cytoplasmic dye (CellBrite Red, Biotium) and imaged with a Cy5 filter set ($\lambda_{ex}/\lambda_{em}$ 644/665 nm) and 300 msec exposure per image or labeled with a live nuclear dye (NucBlue, Invitrogen) and imaged with a DAPI filter set ($\lambda_{ex}/\lambda_{em}$ 358/461 nm) and 200 msec exposure per image. The outline of the central electrode slit was visualized by illumination with the DAPI filter set and a one-time 300 msec exposure. Fluorescence illumination was supplied by a metal halide lamp (xCite 120, EXFO). Images were captured at 10 min intervals.

For experiments assessing proliferation, 5-ethynyl-2’-deoxyuridine (EdU, Invitrogen) was added to the perfusion media at a concentration of 10 μM for the final 6 hours of stimulation

in a given time-course, which lasted up to 12 hours. This 6 hour incubation strategy was used to avoid EdU saturating the tissue. Immediately after the experiment, cells were fixed and permeabilized, then EdU was labeled with Alexa Fluor 488 azide following the manufacturer's protocol (Click-iT EdU Imaging Kit, Invitrogen). Additionally, cell nuclei were labeled with Hoescht 33342 at a concentration of 5 μg/mL for 30 minutes. Cells labeled in this way were imaged on a Nikon Ti2 with a Nikon Qi2 CMOS camera and NIS Elements software. Images for EdU visualization were captured with a GFP filter set at 50% lamp power (SOLA Lumencor, USA) and 400 ms exposure time while images for Hoescht 33342 were captured with a DAPI filter set at 50% lamp power and 500 ms exposure time.

2.6. Image Processing

Tissue velocity maps were generated using PIVLab, a MATLAB script performing FFT-based PIV (Thielicke and Stamhuis, 2014). Iterative window analysis was performed using first 160×160 μm windows followed by 80×80 μm windows, both with 50% step overlap. Vector validation excluded vectors beyond five standard deviations and replaced them with interpolated vectors. Line integral convolution was used to visualize the flow field at certain time points and presented as the flow map. The velocity vector fields were then imported into MATLAB for kymograph generation and plotting. When required, labeled nuclei were tracked using FIJI'S TrackMate plugin set to detect spots via Laplacian of the Gaussian filtering and to link using Linear Motion Tracking (Tinevez et al., 2017).

When counting labeled cells for proliferation analysis, FIJI was used to apply a Gaussian blur to the image, then the Find Maxima function was used to count cells inside a region of interest. The count of the total population labeled by Hoescht 33342 was compared to the number of cells with any level of EdU incorporation to assess the fraction of cells actively proliferating. The tissue bulk regions and center were analyzed separately. Bulk regions of interest, approximately 4.5 mm X 2.5 mm, were selected on either side of the cathode to avoid biases from the edge of the tissue. A central region of interest, approximately 0.25 mm X 2.5 mm, was selected to analyze the high-density tissue directly underneath the cathode.

2.7. Statistical Analysis

Significance of the increase in wound closure rate assessed by EdU labeling was determined by the two-sample t-test, computed in MATLAB with the Statistics and Machine Learning toolbox.

2.8. Data and Enabling Materials availability

All analysis code, device schematics, implementation guides, and validation data will be provided via our updated GitHub repository as listed here: https://qithub.com/CohenLabPrinceton/SCHEEPDOG

3. Results

3.1. Device design for convergent electrical stimulation.

Our new electrobioreactor departs from most extant electrotaxis systems by generating an electric field that converges at the center of model wounds, and functions as follows. The

device consists of an acrylic insert clamped to a standard tissue culture dish, holding electrodes and agarose salt bridges in position (Figure 1A). Three chloridized silver stimulation electrodes (anodes at left and right, cathode at center) are isolated from each other in separate saline reservoirs and electrical contact with the culture media is provided by 4% agarose w/v salt bridges cast inside the insert, one per reservoir (Figure 1B). The ~500 μm thin, laser-milled, agarose bridge serves as a central cathode and is aligned directly over the wound site (Figure 1C, see '*'). The result is a stable, uniform field that converges upon the central electrode as confirmed by simulation (Figure 1D,E).

To reliably generate reproducible tissues and linear wounds, we use a silicone stencil templating method (Cohen et al., 2014; Heinrich et al., 2020) that prepares confluent monolayers the evening before an experiment. We then assemble the electrobioreactor over these tissues prior to imaging. For these experiments, we use layers of keratinocytes from primary skin cultured under basal conditions optimized for electrotaxis (Zajdel et al., 2020). After the tissues have grown, the stencils are removed, and the device is clamped over the cells, aligned such that that the central slit electrode is in the gap between cells (Figure 1E). Then, a computer-controlled source meter (Keithley 2450) is connected to each pair of electrodes (left-center and right-center), with both sources sharing the central cathode, to supply an electric current. The field within the chamber is continuously monitored by a digital oscilloscope and the current output of each source meter is adjusted via closed-loop control to maintain a constant 2 V/cm field strength directed toward the central cathode. We specifically chose this field strength as it has previously been validated and was chosen to amplify the approximate field strength experienced *in vivo* (McCaig et al., 2009). The current density experienced by cells was 0.8-1.0 mA/mm^2. To extend cathode lifetime, only one source was active at a time, alternating between left-center and right-center stimulation every 30 seconds to produce a time-averaged convergent field. While continuous, simultaneous stimulation is effective and results in a roughly 8-10% higher mean edge speed than alternating between each side (see Supplementary Information, Figure S1 for a comparison), our strategy effectively halved the rate of cathode degradation while doubling system lifetime. From a cellular perspective, this strategy is safe as we and others have previously shown that cells still respond to electrical stimuli at lower duty cycles (50-60%) (Ren et al., 2019; Zajdel et al., 2020). Oxygen delivery and waste management are handled by perfusing fresh media through the bioreactor at 2 mL/h, turning over the chamber volume ~11 times per hour. The resulting system provides a robust convergent field to viable cells.

Stable DC stimulation and cell viability require that the electrodes remain intact throughout an entire experiment, so optimization of electrode chemistry is an important consideration. Virtually all DC electrotaxis chambers use an anode and a cathode to inject Faradaic current through a sample, using combinations of salt bridges, media perfusion, and heavy buffering to prevent the build-up of toxic electrochemical by-products or harmful pH changes due to electrolysis at the electrodes (Li et al., 2020; Schopf et al., 2016; Zhao et al., 2014). Because the current used in our device is moderate (~4-6 mA) and the 1.5 mm gap between tissues is relatively large, the central cathode must be able to sink current for an extended period to induce tissue convergence, ideally 12 hours or more. To support this, our system uses electrically chloridized silver foil as electrodes, which degrades at the cathode into ionic

silver and chloride during stimulation. This reaction is more favorable than the hydrolysis cathodal half-reaction, which evolves hydrogen gas from the solution and increases pH (Li et al., 2020). This allows for safe stimulation until AgCl is depleted at the cathode, when evolution of H_2 then becomes favorable and pH increases rapidly, which can cause cytotoxicity. Therefore, sufficient chloridization of the silver foil is paramount for extended electrode lifetime. We compared our chloridization method with bleach immersion, another technique commonly used to chloridize silver. We performed repeated cyclic voltammetry to compare electrode preparations and found that this method of electroplating silver chloride resulted in more stable cathodes (Supplementary Information, Figure S2). While we and several others use electroplating (Kemkemer et al., 2020; Zhao et al., 2014), the majority of the community relies on bleaching, which we found to be unstable and motivated us to provide this characterization to help define new best practices. Our combined approach of robust silver chloridization, agarose diffusion barriers to prevent ionic silver reaching the tissue, and media perfusion integrates numerous best practices in the electrotaxis field to maximize cell viability during stimulation in our device, allowing for extended wound healing experiments.

3.2. Accelerating gap wound closure.

To evaluate this platform for *in vitro* healing, we patterned two 10 x 3 mm tissues spaced 1.5 mm apart with the central cathode aligned over the wound center (Figure 1F). The acrylic outline of the central cathode slit fluoresces weakly when imaged using a standard DAPI filter set, so the alignment between the central cathode and the tissues could be tuned and verified. We then applied convergent electrical stimulation over 12 hours, with striking results (Figure 2, Videos 1 and 2). In the non-stimulated control case, cell proliferation and migration lead to the slow expansion of tissues and gradual, but incomplete closure of the wound over 12 hours (~50% closure, N=3). However, convergent bioelectric stimulation led to complete closure between 11-12 h (N=3). More specifically, the edge migration speed was twice as fast in the stimulated case as in the control, measuring 29.4 ± 3.3 μm/h and 61.0 ± 7.9 μm/h for the control and stimulated cases, respectively. The two-sample t-test was performed on the edge speeds (N=6 edges for each condition) to determine that this difference is statistically significant ($p = 4 \times 10^{-6}$). To conclusively attribute this effect to electrical stimulation rather than temperature effects (Joule heating has been linked to increased migration speeds in prior studies (Allen et al., 2013; Ream et al., 2003)) we monitored the device temperature during stimulation (Figure S3). The steady state temperature in the bioreactor only rose from 37±0.5 °C to 38±0.5 °C over the experiment. This 1 °C (3%) increase in incubation temperature is unlikely to account for ~2X increase in migration speed during stimulation, especially given prior work relating temperature to migration during electrotaxis (Allen et al., 2013). We hypothesize that perfusion and media turn over helps to exchange heat and mitigate any effects from Joule heating. Taken together, this is the first demonstration of convergent field stimulation accelerating *in vitro* wound healing to millimeter-scale gap closure, and the results prove that electrotaxis alone is sufficient for this acceleration.

3.3. Driven collective migration during healing.

To better characterize device performance and its effects on large scale tissue growth and motion, we performed particle image velocimetry (PIV) on each tissue. Representative horizontal velocity kymographs for both the control and convergent stimulation cases are shown in Figure 3 (compare with Video 1). To provide context of spatial dynamics within a given tissue, we show representative heatmaps of horizontal velocity and line integral convolution (LIC) migration maps to visualize the overall flow of cellular motion at 4 hours after the onset of stimulation (steady state). Throughout the control tissue (Figures 3A-C), there is little net outwards motion, except for slow expansion at the edges. Disorder is apparent in the velocity and migration maps of the control tissues, which lack large regions of coordinated movement, as expected for non-stimulated tissues (Figures 3B,C). In contrast, bioelectric stimulation resulted in nearly uniformly high-speed motion throughout the tissue, converging on the gap within 15 minutes of the field turning on, as visualized in the velocity and migration maps (Figures 3D-F). The large number of parallel streaklines along the stimulation direction in the migration map demonstrates highly coordinated motion across the tissue in alignment with the stimulus (Figures 3F). These visualizations reveal that the electric field acts a global migration cue across a large area, confirming that cells experience a highly uniform field as predicted by simulation (Figure 1D,E).

3.4. Convergent migration near the field singularity.

Having demonstrated that the *in vitro* healing process can be electrically accelerated overall, we next characterized cellular responses specifically during the final stages of wound closure. Unlike traditional electrotaxis chambers where the electrodes are significantly distal to the tissue to ensure a uniform field, our healing-on-a-chip device requires a central electrode to focus cell migration into the wound zone. Since the central electrode has a finite width (~500 μm here) that is smaller than the wound, tissues will eventually pass underneath the electrode and enter the ‘electrode shadow’ during the final stages of healing and convergence. Any discrete electrode produces field non-uniformities close to its surface, so as cells enter the electrode shadow, they will experience a very different field than out in the fully developed zones far from the center. Our simulation predicts a sharp decrease in electric field strength that begins about 500 μm on either side of the central cathode above the convergence region (Figure 4A). We quantified the actual effects of the central field singularity by stimulating closed tissues for 6 hours and using a live nuclear dye to track cells in that central zone (Video 3). We averaged PIV across the region surrounding the closure zone over the stimulation period (Figure 4B, asterisks and error bars) and fit a sigmoid function to the data (Figure 4B, inset) showing that there is a strong, steady-state response far from the central electrode that steadily weakens as cells approach the central electrode and enter the electrode shadow (Figure 4, dashed blue line; magenta zone shows electrode shadow). While this local weakening of the electrotactic response closely resembled the trend in our simulations, cells nonetheless continued to directionally migrate deep into the electrode shadow zone, only to dropping to <50% of the steady state velocity once cells were ~100 μm off the electrode midline. These data show that the effective electrode size is smaller than its physical, 500 μm width (Figure 4B, compare dotted black boundaries to electrode boundaries), suggesting that even relatively large electrodes can still promote last-mile healing.

We suggest two reasons for why the ‘effective electrode’ size would be smaller than its physical size. First, the threshold field strength that elicits an electrotaxis response is lower than the 2 V/cm we target in stimulation. As the field strength rolls off, it is still ‘therapeutic’ for some distance, given that physiological field strengths are on the order of 1 V/cm (McCaig et al., 2009). Second, the monolayers carry some memory of the electrotaxis response that continues to influence their responses after the stimulus changes (Ren et al., 2019; Zajdel et al., 2020). Keratinocytes polarize in response to the field stimulus, and this polarization takes time to decay once a stimulus is no longer detected. This could lead to cells effectively coasting, unguided, during the last gap before tissue closure.

3.5. Risks and significance of continued stimulation post gap-healing.

Critically, we also observed potential consequences to continued electrical stimulation after a wound had closed. As has been noted previously (Ream et al., 2003), electrotaxis appears to override basic cellular safety mechanisms such as contact inhibition, so cells will continue trying to directionally migrate as long as stimulation is active. In our wound healing model, stimulating after a tissue had closed would continue to drive cell migration towards where the center of the wound had previously been. This inevitably caused an increase in local cell density, and we measured a >2X increase (from 750 to 1600 cells/mm^2) in cell density under the electrode shadow relative to density distal to the central electrode (Figure 4C-E), showing there is potential for a high-density zone to build up due to continued post-healing stimulation that could potentially alter the healing process such as by overconcentrating cells within the wound bed or potentially altering scar formation *in vivo* (Oliveira et al., 2019). Comparing individual cell trajectories within the central zone confirmed that cells within the electrode shadow horizontally translated a shorter distance than those that were farther away (Figure 4F,G). This reduction in overall translation extended, in a graded fashion, outwards 500 μm from the center in either direction, consistent with the reduction of speed cells experience as they enter the electrode shadow. Nevertheless, there is net migration towards the center, even for cells that were initially positioned under the electrode, suggesting again that the electrode’s influence extends underneath its width despite significant weakening of the effective field strength.

3.6. Extended stimulation effects on cell cycle progression

Since cell migration and proliferation are both affected by cell density, we characterized the time course of cell cycle progression during stimulation by assaying EdU incorporation (Yu et al., 2009). An increase or decrease in the rate of EdU uptake indicates a corresponding change in DNA synthesis, and we analyzed central and bulk regions separately. We observed a significant decrease in the proliferation rates in stimulated tissue bulks (far from the cathode) starting at 3 hours that continued onwards to 12 hours (Supplementary Information, Figure S4), with the overall proliferation rate dropping from ~55% to ~23%, relative to ~53% to ~49% for the control. This reduction is consistent with prior studies that demonstrate a similar effect of DC stimulation (Ren et al., 2019; Wang et al., 2003). More surprisingly, we observed a transient increase in proliferation rate immediately underneath the cathode where the electric field converged for the first 6 hours of stimulation. This is unexpected since the local increase in cell density might have led to contact inhibition. We hypothesize that the local environment underneath the electrode may differ significantly

from conditions in the bulk in terms of local current density and ion fluxes, which might have significant and unexpected impacts on proliferation during the onset of stimulation. These results suggest that more thorough study of the effects of electrical stimulation on proliferation is warranted, and that other stimulation schemes such as pulsed DC or AC might have complementary effects for wound healing. More specifically, these results highlight the importance of considering electrode/cell proximity as a design variable.

4. Discussion

Overall, we present a bioelectric, healing-on-a-chip (HoC) platform designed specifically to study the role of electrotaxis and other electrical phenomena in wound healing. Unique for electrical stimulation bioreactors, our approach creates a field stimulation pattern that mimics that found in wounds in vivo, with the field converging at the center of the wound gap. This capability allows us to directly explore the actual healing process, rather than purely unidirectional cell migration. Therefore, our platform allows study of the *in vitro* healing process spanning initial injury, 'first contact' as the sides of the wound meet and, critically, post-closure behavior after the wound has healed. Using this platform and unoptimized stimulation parameters, we demonstrate ~2X acceleration of wound closure in an *in vitro* skin layer model due solely to electrotactic effects. This demonstration visualizes the effect of electrotaxis itself accelerating the healing process, expanding upon prior convergent stimulation work (Sun et al. 2012) to demonstrate complete, accelerated closure millimeter-scale gap wounds for the first time. The stability, reproducibility, and programmability of the platform make it suitable to deeply explore key technological and biological questions, and we have taken care to ensure the device is easily replicable and accessible to a broad audience.

That even naïve stimulation had a strong, positive effect on *in vitro* healing is encouraging, and establishes a clear baseline against which future parameter optimization studies can be compared. This approach could be critical to the community as standardization and optimization of stimulation approaches remains an open question. To address this, we explored the effects of stimulating beyond initial closure of the wound by electrically stimulating a closed tissue, and the resulting cellular pile-up indicates both the potency of electrotaxis to drive migration and the importance of being able to fine-tune and intelligently adjust stimulation in practice to avoid detrimental effects of overstimulation. Such cellular pile-ups also speak more fundamentally to the role of electrotaxis as a tool to modulate and explore interactions at the boundaries between tissues.

Because tight coupling between cell cycle progression and cell migration has been demonstrated (Molinie et al., 2019), we studied the effect of prolonged stimulation on proliferation via an EdU incorporation assay. Our brief survey showed reduced proliferation in both the bulk and cathode region starting after extended stimulation, but also unexpectedly showed an increase in proliferation rate directly under the cathode during the onset of stimulation. This increase suggests potential changes in the ionic environment at an electrode directly over tissues has implications for the dynamics of the cell cycle. Additional studies of the dynamics of proliferation directly under a stimulation electrode would also

work towards the understanding required to better prescribe stimulation programs for optimal healing.

While we specifically investigated healing in monolayers of primary skin cells in this study, in principle, any adherent cell type is compatible with this system. We used the primary mouse keratinocyte skin layer model as it is a standard model in the field and allowed us to place our work in the context of other studies. Wound healing *in vivo* clearly involves complex coordination across multiple cell types (e.g. macrophages and immune cells, fibroblasts, and vascular cells, and epidermal cells) and phases, (e.g. inflammation, granulation, and re-epithelialization) (Tai et al., 2018). That our platform supports pre-engineering tissue configurations means that co-cultures or more complex tissue models can be grown first and then incorporated into the bioreactor to allow more complex studies on healing. When linked to stimulation optimization approaches, it may be possible to determine modalities that preferentially target a given cell type, or process such as proliferation vs. migration during healing. Again, these questions benefit from a field geometry that enables a healing phenotype.

We look forward to the translation of our findings, and those of others in this space, into therapeutic applications in wound healing, both for acute and chronic wounds. Having confirmed the power of direct current stimulation to produce safe, strong directed cellular migration, future research would include testing the stimulation on more complex, 3D models as well as scaling up our technology to cover larger wounds than presented here. Recently developed therapeutic electrical appliances are on the scale of ~10 cm (Kloth, 2014; Ovens, 2014), which is sufficient size to cover a small ulcer wound, suggesting it is possible to scale up the stimulation geometry in this paper to cover real-life wounds in patients.

5. Conclusions

Our bioelectric ‘Healing-on-a-Chip’ approach is fully open and intended to be modified and tailored for a variety of applications. We provide complete design files, computational models, and stimulation code, and the basic approach lends itself to easy customization. For instance, electrode shape, size, number, and location can easily be adjusted without additional cost or significant complexity. Field stimulation strategies can be tested by attaching any desired power supplies or running arbitrary stimulation code to activate electrode sequences. Our autofluorescence alignment approach makes it possible to accurately align a given electrode configuration to a given wound and removes much of the ambiguity and difficulty this process would normally introduce. We hope the demonstrations here and flexibility of the device can help accelerate healing-on-a-chip research, improve translation for future *in vivo* applications, and even support new, research on general interactions between colliding tissues.

Supplementary Material

Refer to Web version on PubMed Central for supplementary material.

Acknowledgments

We gratefully acknowledge Prof. Danelle Devenport and Katie Little at Princeton University for providing primary keratinocytes and culture support. Portions of the research reported in this publication was supported by the National Center for Advancing Translational Sciences (NCATS), a component of the National Institutes of Health (NIH) under award number TL1TR003019 (TJZ). Further support was provided by National Institutes of Health grant R35GM13357401 (DJC), and National Science Foundation CAREER: 2046977 (DJC, GS). The content is solely the responsibility of the authors and does not necessarily represent the official views of the National Institutes of Health or the National Science Foundation.

References

ACP, 2017. Accelerate Wound Healing with ACP's Wound Management Program. Accelerated Care Plus Corporation.

Allen GM, Mogilner A, Theriot JA, 2013. Electrophoresis of cellular membrane components creates the directional cue guiding keratocyte galvanotaxis. Current Biology23, 560–568. [PubMed: 23541731]

Anderson CA, Hare MA, Perdrizet GA, 2016. Wound healing devices brief vignettes. Advances in wound care5, 185–190. [PubMed: 27076996]

Ashrafi M, Alonso-Rasgado T, Baguneid M, Bayat A, 2017. The efficacy of electrical stimulation in lower extremity cutaneous wound healing: a systematic review. Experimental dermatology26, 171–178. [PubMed: 27576070]

du Bois-Reymond E, 1848. Untersuchungen uber thierische Elektricitat. Berlin, Reimer1.

Cohen DJ, Nelson WJ, Maharbiz MM, 2014. Galvanotactic control of collective cell migration in epithelial monolayers. Nature materials13, 409–417. [PubMed: 24608142]

Cortese B, Palama IE, D'Amone S, Gigli G, 2014. Influence of electrotaxis on cell behaviour. Integrative Biology6, 817–830. [PubMed: 25058796]

Franek A, Kostur R, Polak A, Taradaj J, Szlachta Z, Blaszczak E, Dolibog P, Dolibog P, Koczy B, Kucio C, 2012. Using high-voltage electrical stimulation in the treatment of recalcitrant pressure ulcers: results of a randomized, controlled clinical study. Ostomy-Wound Management58, 30.

Gokoffski KK, Jia X, Shvarts D, Xia G, Zhao M, 2019. Physiologic electrical fields direct retinal ganglion cell axon growth in vitro. Investigative ophthalmology & visual science60, 3659–3668. [PubMed: 31469406]

Haesler E, 2014. National Pressure Ulcer Advisory Panel, European Pressure Ulcer Advisory Panel and Pan Pacific Pressure Injury Alliance. Prevention and Treatment of Pressure Ulcers: Quick Reference Guide. Cambridge Media, Perth, Australia.

Heinrich MA, Alert R, LaChance JM, Zajdel TJ, Košmrlj A, Cohen DJ, 2020. Size-dependent patterns of cell proliferation and migration in freely-expanding epithelia. eLife9, e58945. 10.7554/eLife.58945 [PubMed: 32812871]

Hunckler J, De Mel A, 2017. A current affair: electrotherapy in wound healing. Journal of multidisciplinary healthcare10, 179. [PubMed: 28461755]

Isseroff RR, Dahle SE, 2012. Electrical stimulation therapy and wound healing: where are we now? Advances in wound care1,238–243. [PubMed: 24527312]

Jang HK, Oh JY, Jeong GJ, Lee TJ, Im GB, Lee JR, Yoon JK, Kim DI, Kim BS, Bhang SH, Lee TI, 2018. A disposable photovoltaic patch controlling cellular microenvironment for wound healing. International Journal of Molecular Sciences19. 10.3390/ijms19103025

Kai H, Yamauchi T, Ogawa Y, Tsubota A, Magome T, Miyake T, Yamasaki K, Nishizawa M, 2017. Accelerated Wound Healing on Skin by Electrical Stimulation with a Bioelectric Plaster. Advanced Healthcare Materials6, 1–5. 10.1002/adhm.201700465

Kemkemer R, Naggay BK, Schmidt TB, Ende K, 2020. Development of a multi-well-chip for studying 2D and 3D tumor cell migration and spheroid growth in electrical fields. Current Directions in Biomedical Engineering6, 164–167.

Kennard AS, Theriot JA, 2020. Osmolarity-independent electrical cues guide rapid response to injury in zebrafish epidermis. Elife9, e62386. [PubMed: 33225997]

Khouri C, Kotzki S, Roustit M, Blaise S, Gueyffier F, Cracowski J-L, 2017. Hierarchical evaluation of electrical stimulation protocols for chronic wound healing: An effect size meta-analysis. Wound Repair and Regeneration25, 883–891. [PubMed: 29052946]

Kloth LC, 2014. Electrical stimulation technologies for wound healing. Advances in wound care3, 81–90. [PubMed: 24761348]

Kloth LC, 2005. Electrical stimulation for wound healing: a review of evidence from in vitro studies, animal experiments, and clinical trials. The international journal of lower extremity wounds4, 23–44. [PubMed: 15860450]

Li M, Wang X, Rajagopalan P, Zhang L, Zhan S, Huang S, Li W, Zeng X, Ye Q, Liu Y, others, 2020. Toward Controlled Electrical Stimulation for Wound Healing Based on a Precision Layered Skin Model. ACS Applied Bio Materials.

Liang Y, Tian H, Liu J, Lv YL, Wang Y, Zhang JP, Huang YS, 2020. Application of stable continuous external electric field promotes wound healing in pig wound model. Bioelectrochemistry135, 107578. 10.1016/j.bioelechem.2020.107578 [PubMed: 32534380]

Long Y, Wei H, Li J, Yao G, Yu B, Ni D, Gibson AL, Lan X, Jiang Y, Cai W, Wang X, 2018. Effective Wound Healing Enabled by Discrete Alternative Electric Fields from Wearable Nanogenerators. ACS Nano12, 12533–12540. 10.1021/acsnano.8b07038 [PubMed: 30488695]

Martinengo L, Olsson M, Bajpai R, Soljak M, Upton Z, Schmidtchen A, Car J, Järbrink K, 2019. Prevalence of chronic wounds in the general population: systematic review and meta-analysis of observational studies. Annals of epidemiology29, 8–15. [PubMed: 30497932]

McCaig CD, Rajnicek AM, Song B, Zhao M, 2005. Controlling cell behavior electrically: current views and future potential. Physiological reviews.

McCaig CD, Song B, Rajnicek AM, 2009. Electrical dimensions in cell science. Journal of cell science122, 4267–4276. [PubMed: 19923270]

Molinie N, Rubtsova SN, Fokin A, Visweshwaran SP, Rocques N, Polesskaya A, Schnitzler A, Vacher S, Denisov EV, Tashireva LA, others, 2019. Cortical branched actin determines cell cycle progression. Cell research29, 432–445. [PubMed: 30971746]

Morris C, 2006. Bio-electrical stimulation therapy using POSiFECT®RD. WoundsUK2, 112–116.

Oliveira K, Barker J, Berezikov E, Pindur L, Kynigopoulos S, Eischen-Loges M, Han Z, Bhavsar M, Henrich D, Leppik L, 2019. Electrical stimulation shifts healing/scarring towards regeneration in a rat limb amputation model. Scientific reports9, 1–14. [PubMed: 30626917]

Ovens L, 2014. Electroceutical therapy to manage complex leg ulcers: a case series of three patients. WoundsUK10.

Padula WV, Delarmente BA, 2019. The national cost of hospital-acquired pressure injuries in the United States. International Wound Journal16, 634–640. 10.1111/iwj.13071 [PubMed: 30693644]

Ream RA, Theriot JA, Somero GN, 2003. Influences of thermal acclimation and acute temperature change on the motility of epithelial wound-healing cells (keratocytes) of tropical, temperate and Antarctic fish. Journal of experimental biology206, 4539–4551.

Ren X, Sun H, Liu J, Guo X, Huang J, Jiang X, Zhang Y, Huang Y, Fan D, Zhang J, 2019. Keratinocyte electrotaxis induced by physiological pulsed direct current electric fields. Bioelectrochemistry127, 113–124. 10.1016/j.bioelechem.2019.02.001 [PubMed: 30818261]

Schopf A, Boehler C, Asplund M, 2016. Analytical methods to determine electrochemical factors in electrotaxis setups and their implications for experimental design. Bioelectrochemistry109, 41–48. [PubMed: 26775205]

Shen Y, Pfluger T, Ferreira F, Liang J, Navedo MF, Zeng Q, Reid B, Zhao M, 2016. Diabetic cornea wounds produce significantly weaker electric signals that may contribute to impaired healing. Scientific Reports6,1–12. 10.1038/srep26525 [PubMed: 28442746]

Sun Y-S, Peng S-W, Cheng J-Y, 2012. In vitro electrical-stimulated wound-healing chip for studying electric field-assisted wound-healing process. Biomicrofluidics6, 034117.

Tai G, Tai M, Zhao M, 2018. Electrically stimulated cell migration and its contribution to wound healing. Burns & trauma6.

Thielicke W, Stamhuis E, 2014. PIVlab–towards user-friendly, affordable and accurate digital particle image velocimetry in MATLAB. Journal of open research software2.

Tinevez J-Y, Perry N, Schindelin J, Hoopes GM, Reynolds GD, Laplantine E, Bednarek SY, Shorte SL, Eliceiri KW, 2017. TrackMate: An open and extensible platform for single-particle tracking. Methods115, 80–90. [PubMed: 27713081]

Ud-Din S, Bayat A, 2014. Electrical stimulation and cutaneous wound healing: a review of clinical evidence, in: Healthcare. Multidisciplinary Digital Publishing Institute, pp. 445–467.

Wahlsten O, Skiba JB, Makin IRS, Apell SP, 2016. Electrical field landscape of two electroceuticals. Journal of Electrical Bioimpedance7, 13–19. 10.5617/jeb.2693

Wang E, Yin Y, Zhao M, Forrester JV, McCaig CD, 2003. Physiological electric fields control the G1/S phase cell cycle checkpoint to inhibit endothelial cell proliferation. The FASEB journal17, 1–14. [PubMed: 12522106]

Wang X-F, Li M-L, Fang Q-Q, Zhao W-Y, Lou D, Hu Y-Y, Chen J, Wang X-Z, Tan W-Q, 2020. Flexible electrical stimulation device with Chitosan-Vaseline® dressing accelerates wound healing in diabetes. Bioactive materials6, 230–243. [PubMed: 32913931]

Wang Z, Samanipour R, Koo K, Kim K, 2015. Organ-on-a-chip platforms for drug delivery and cell characterization: A review. Sens. Mater27, 487–506.

Yu C, Xu ZX, Hao YH, Gao YB, Yao BW, Zhang J, Wang B, Hu ZQ, Peng RY, 2019. A novel microcurrent dressing for wound healing in a rat skin defect model. Military Medical Research6, 1–9. 10.1186/s40779-019-0213-x [PubMed: 30678725]

Yu Y, Arora A, Min W, Roifman CM, Grunebaum E, 2009. EdU incorporation is an alternative non-radioactive assay to [3H] thymidine uptake for in vitro measurement of mice T-cell proliferations. Journal of immunological methods350, 29–35. [PubMed: 19647746]

Zajdel TJ, Shim G, Wang L, Rossello-Martinez A, Cohen DJ, 2020. SCHEEPDOG: Programming Electric Cues to Dynamically Herd Large-Scale Cell Migration. Cell Systems10, 506–514.e3. 10.1016/j.cels.2020.05.009 [PubMed: 32684277]

Zhang B, Korolj A, Lai BFL, Radisic M, 2018. Advances in organ-on-a-chip engineering. Nature Reviews Materials3, 257–278.

Zhang B, Radisic M, 2017. Organ-on-a-chip devices advance to market. Lab on a Chip17, 2395–2420. [PubMed: 28617487]

Zhao S, Zhu K, Zhang Y, Zhu Z, Xu Z, Zhao M, Pan T, 2014. ElectroTaxis-on-a-Chip (ETC): An integrated quantitative high-throughput screening platform for electrical field-directed cell migration. Lab on a Chip14, 4398–4405. 10.1039/c4lc00745j [PubMed: 25242672]

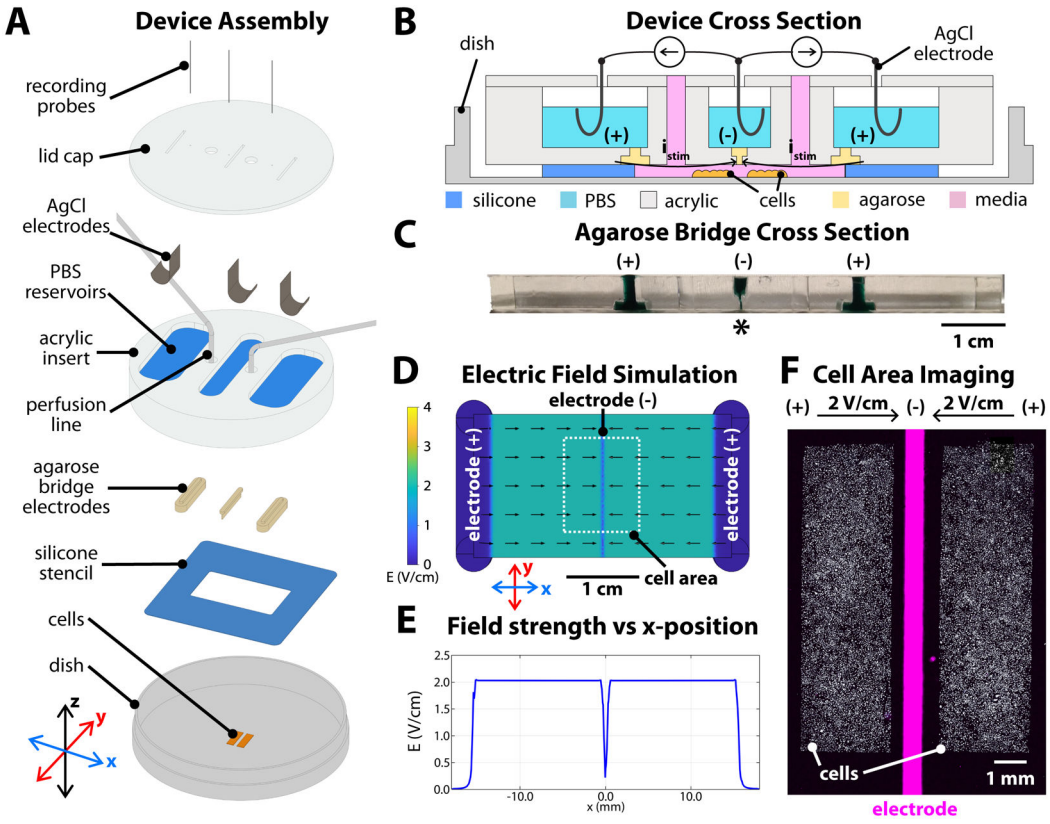

Figure 1.

Convergent field stimulation device. (A) Layer-based assembly of the bioreactor onto a tissue culture dish. Cells are patterned in the center of the dish, then a 250 μm-thick silicone stencil is placed to define the stimulation area and height. Agarose bridges are cast inside an acrylic insert, then clamped into the dish and against the silicone stencil. The reservoirs on the topside of the acrylic insert are filled with phosphate-buffered saline (PBS). Chloridized silver electrodes and titanium wire recording probes are inserted in each reservoir, all held in place by a lid cap. (B) Device cross-section sketch and (C) photograph of the sectioned agarose bridges stained with green food coloring for contrast. The narrow cathode is labelled with '*'. (D) Numeric simulation of the electric field in the device, showing constant 2 V/cm field strength converging toward the center, with a steep drop-off in strength starting ±500 μm from the center. (E) Simulated field strength versus x-position in the device. (F) Microscope capture of the central area of the assembled device, showing the central electrode 500 μm wide positioned between the two tissues. The cells (white) were labelled with a Cy5 lipophilic dye and the outline of the central electrode was visualized with a DAPI filter set (λ_{ex}/ λ_{em} 358/461 nm) and filled via post-processing in ImageJ (magenta).

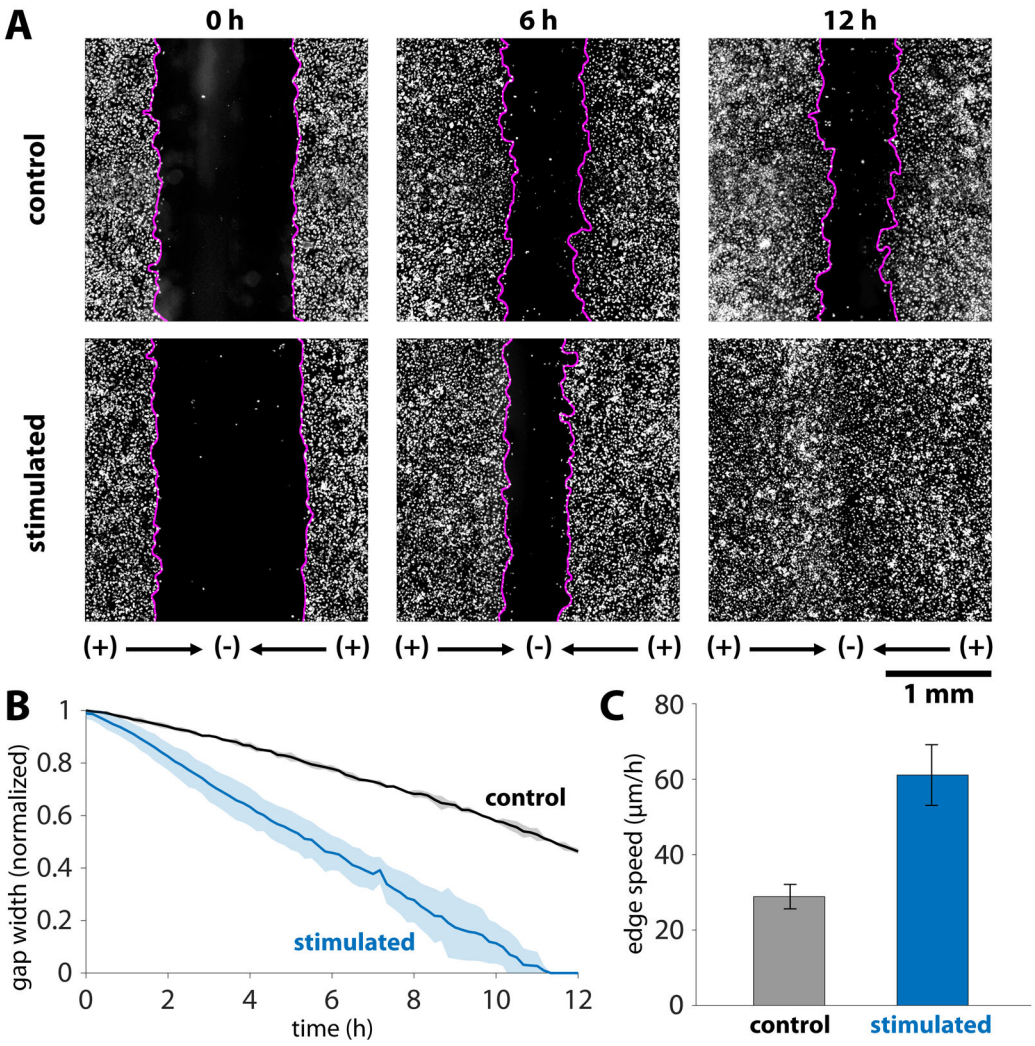

Figure 2.

Dynamics of accelerated wound closure of keratinocyte monolayers. (A) Timepoint comparison of stimulation versus control for keratinocytes labelled with a Cy5 cytoplasmic dye. Gap boundaries are demarked by magenta lines. Initial gap between tissues was 1.5 mm, and this gap closed by 12 hours in the stimulated case, while roughly 50% of the gap remained in the control case. (B) Gap closure normalized to the initial gap width for N = 3 tissues in each condition. Shaded region represents one standard deviation. (C) Edge expansion speeds averaged over an 8 h period. The average edge expansion was 29.4 ± 3.3 μm/h and 61.0 ± 7.9 μm/h for the control and stimulated cases, respectively. Error bars represent standard deviation (N=6 edges in each condition). There is a statistically significant increase in edge speed when stimulated as determined by the two-sample t-test ($p = 4 \times 10^{-6}$).

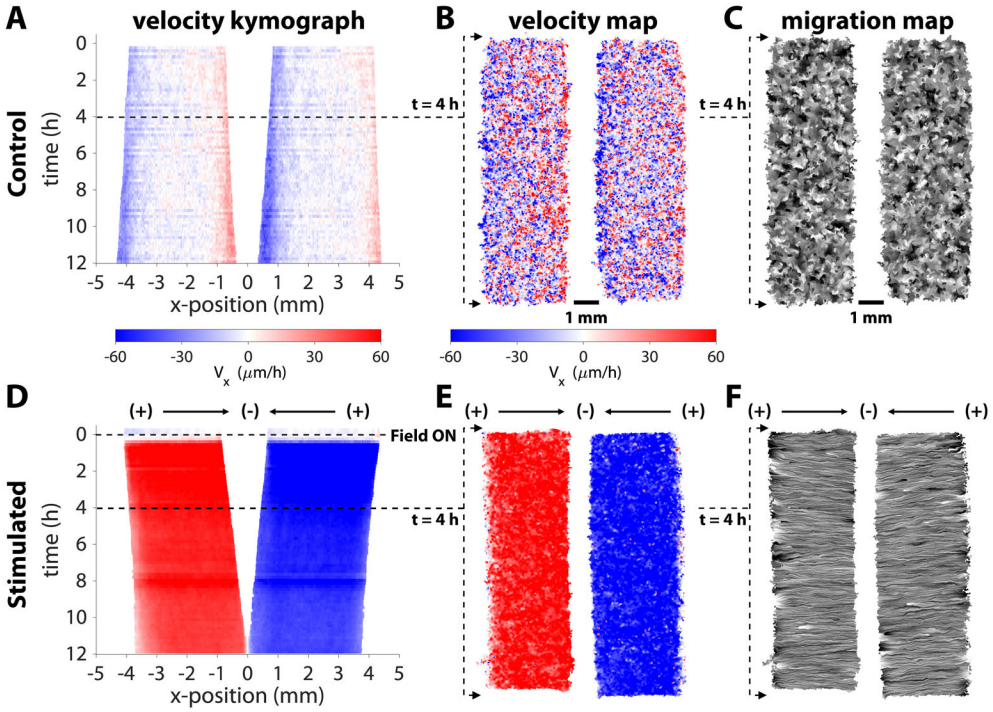

Figure 3.

Convergent stimulation results in coherent migration response towards the center. Representative kymograph of V_x averaged across x-position in a control (A) and stimulated (D) tissue pair. The control tissues expand uniformly outwards, while the stimulated tissues converge towards the cathode with uniformly high speed across the tissue area (~60 μm/h directed towards the gap). Horizontal velocity maps (B,E) and migration maps (C,F) in representative tissue pairs.

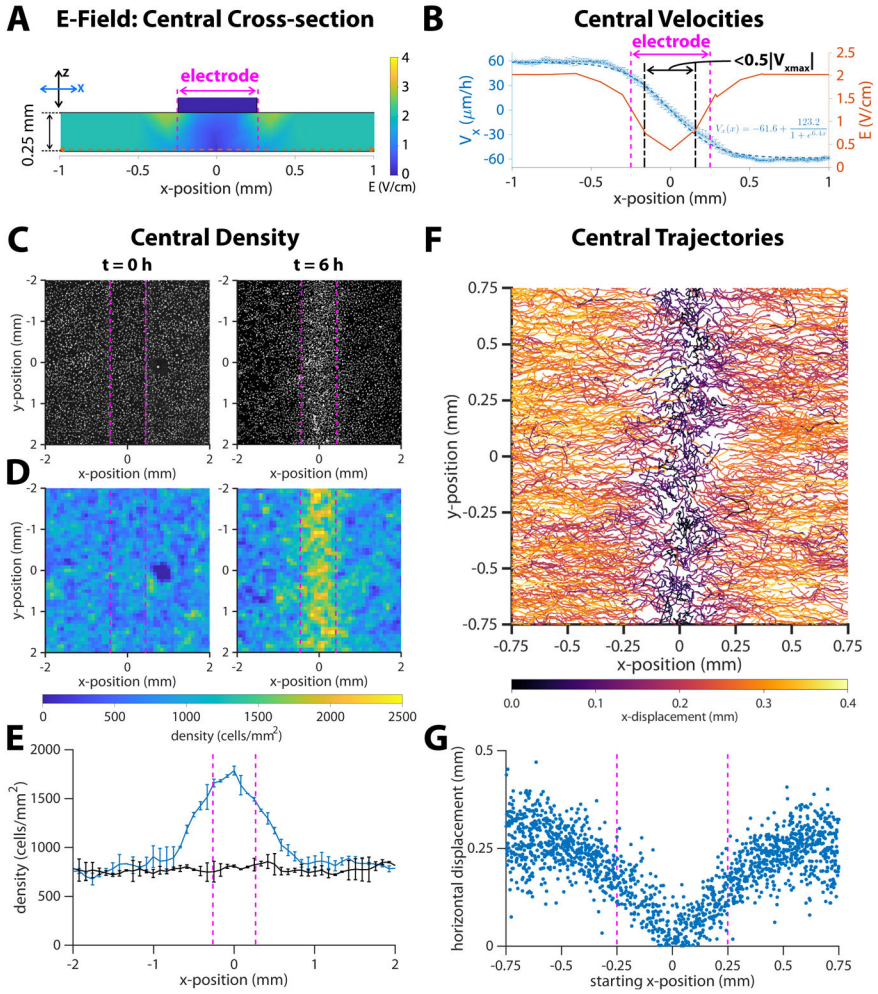

Figure 4.

Response of migrating cells near the center of a closed tissue. Dotted vertical magenta lines indicate approximate cathode boundaries in each respective graph. (A) Numeric simulation results for the electric field of the channel in cross section. The horizontal dotted line is the section of the electric field plotted in the next panel. (B) Average horizontal velocity plotted as blue *'s with error bars representing standard deviation (N = 2). The dashed blue line indicates a least-squares fit of a sigmoid function to the data, and the formula for this fit is inset in the lower right quadrant of the plot. The region where the horizontal velocity's magnitude drops to < 50% of the steady state value is marked by dot- dash black lines. Predicted strength from numeric simulation (reproduced from Figure 1E) is plotted as a red solid line. (C) DAPI images of cell nuclei and (D) density maps for tissues at the onset of stimulation (t = 0 h) and after six hours of stimulation (t = 6 h). (E) Average cell density versus x-position, where x = 0 is the center of the cathode. Error bars represent standard deviation (N = 2). (F) Montage of 6-hour trajectories of individual cells in proximity with the center. Each track is coloured by net x-displacement. (G) Total horizontal displacement of cell versus its starting x-position relative to the center of the cathode at x = 0.